SARS-CoV-2 NSP13 interacts with TEAD to suppress Hippo-YAP signaling

Fansen Meng[1], Jong Hwan Kim[2], Chang-Ru Tsai[3], Jeffrey D. Steimle[3], Jun Wang[2], Yufeng Shi[2], Rich G. Li[1], Bing Xie[3], Vaibhav Deshmukh[3], Shijie Liu[4, 5], Xiao Li[1], James F. Martin[1,2,3*]

[1]McGill Gene Editing Lab, The Texas Heart Institute, Houston, Texas, United States; [2]Cardiomyocyte Renewal Laboratory, The Texas Heart Institute, Houston, Texas, United States; [3]Department of Integrative Physiology, Baylor College of Medicine, Houston, Texas, United States; [4]The Heart Institute, Division of Molecular Cardiovascular Biology, Cincinnati Children's Hospital Medical Center, Cincinnati, OH, United States; [5]Department of Pediatrics, University of Cincinnati College of Medicine, Cincinnati, OH, United States

[*]**For correspondence:** James F. Martin. Tel: +1 713 798 5931, e-mail: jfmartin@bcm.edu

Competing interest: J.F.M is a founder and owns shares in Yap therapeutics. J.F.M. is a co-inventor on the following patents associated with this study: patent no. US20200206327A1 entitled "Hippo pathway deficiency reverses systolic heart failure post-infarction," patent no.15/642200.PCT/US2014/ 069349 101191411 entitled "Hippo and dystrophin complex signaling in cardiomyocyte renewal," and patent no. 15/102593.PCT/US2014/069349 9732345 entitled "Hippo and dystrophin complex signaling in cardiomyocyte renewal."

Abstract The Hippo pathway is critical to organ development, homeostasis, and regeneration, facilitated by YAP/TEAD-mediated gene expression. Although emerging studies report Hippo-YAP dysfunction after viral infection, it is largely unknown in the context of severe acute respiratory syndrome coronavirus 2 (SARS-CoV-2). Here, we analyzed RNA sequencing data from SARS-CoV-2 infected human lung samples and induced pluripotent stem cell–derived cardiomyocytes (iPSC-CMs), and observed a decrease in YAP target gene expression. In screening SARS-CoV-2 nonstructural proteins, we found that nonstructural protein 13 (NSP13), a conserved coronavirus helicase, inhibited YAP transcriptional activity independent of the upstream Hippo kinases LATS1/2. Consistently, introducing NSP13 into cardiomyocytes suppressed active YAP (YAP5SA) *in vivo*. Subsequent investigations on NSP13 mutants indicated that NSP13 helicase activity is crucial for suppressing YAP transactivation. Mechanistically, TEAD4 serves as a platform for recruiting NSP13 and YAP. NSP13 inactivates the YAP/TEAD4 transcription complex through its interacting proteins, such as transcription termination factor 2 (TTF2). These discoveries reveal a novel YAP/TEAD regulatory mechanism orchestrated by TEAD4, which provides molecular insights of Hippo-YAP regulation after SARS-CoV-2 infection.

Keywords:

NSP13; YAP; TEAD4; SARS-CoV-2; Helicase; Hippo pathway; TTF2

Introduction

The evolutionarily conserved Hippo-YAP signaling pathway integrates various extracellular signals, including mechanical force, cell adhesion, and nutrient availability, through the protein kinases LATS1/2 (*1*). As the primary substrate of LATS kinases, YAP is inactivated after phosphorylation via cytoplasmic retention or degradation. The unphosphorylated YAP translocates to the nucleus and forms complexes with transcription factor partners, notably TEAD, to activate target genes (*1,2*) that are involved in tissue development, homeostasis, and regeneration across multiple organs (*2-7*). YAP/TEAD transactivation is regulated by intricate molecular mechanisms that govern YAP/TEAD activity, localization, and interaction. Dysregulation of these processes has been implicated in various diseases including cancer (*8-11*).

Recent studies have shown that YAP acts as a natural inhibitor of innate immunity against viral infection (*12,13*), but conflicting findings were observed in YAP regulation including expression, degradation, and nucleus localization, after multiple types of viral infection (*14*). Although these observations shed light on the complex dynamics of YAP during viral responses, the specific mechanisms underlying YAP/TEAD regulation after SARS-CoV-2 infection are poorly understood. SARS-CoV-2, which caused the global COVID-19 pandemic, has well-documented effects on the respiratory, digestive, central nervous, and cardiovascular systems (*15-17*). Studying the effects of SARS-CoV-2 on Hippo-YAP signaling provides insight into the molecular underpinnings of virus–induced pathophysiology. Two recent studies showed opposite YAP activity after SARS-CoV-2 infection (*18,19*), but the lack of YAP/TEAD target gene expression data prevented a better understanding of these disparate results. Thus, the precise understanding of YAP/TEAD regulation after SARS-CoV-2 infection remains elusive.

Here, we found that SARS-CoV-2 infection reduced YAP target gene expression in lung epithelial cells of patients with COVID-19 and human induced pluripotent stem cell–derived cardiomyocytes (hiPSC-CMs). Using a comprehensive screening of SARS-CoV-2 nonstructural proteins, we identified NSP13 as a key factor in inhibiting YAP transcriptional activity and suppressing active YAP (YAP5SA) activity *in vivo*. Moreover, NSP13 suppression on YAP was dependent on its helicase activity. Mechanistically, NSP13 directly bound to TEAD4 and inhibited the transcriptional activity of the YAP/TEAD4 complex by recruiting transcriptional suppressors such as TTF2. These findings indicate a novel function of NSP13 in regulating YAP/TEAD activity and provide key insights into how the SARS-CoV-2 genome modulates transcriptional activity of the YAP-TEAD complex.

Results

SARS-CoV-2 infection suppresses YAP activity in host cells

To assess alterations in YAP activity with SARS-CoV-2 infection *in vivo*, we integrated and reanalyzed single nuclei RNA (snRNA) sequencing data derived from human lung samples (*20,21*), identifying 10 major cell types (Figure 1A, figure supplement 1A). The expression levels of TMPRSS2 and ACE2, two key entry factors for SARS-CoV-2 infection (*22*), was higher in lung epithelial cells than in other cell types (Figure 1B, figure supplement 1B). Lung epithelial cells were categorized into alveolar type 1 (AT1) and alveolar type 2 (AT2) (figure supplement 1C, D). SARS-CoV-2 is more likely to infect AT1 cells because they cover >95% of the alveolar surface. The YAP score, evaluated by using 38 YAP target genes expression, was lower in AT1 cells from COVID-19 patients than from controls (Figure 1C). The signature genes associated with AT1 cells including *AGER* and *CLIC5*, reported as YAP target genes (*23,24*), were downregulated in lung

samples from COVID-19 patients (figure supplement 1E). To substantiate this phenotype, we evaluated a bulk RNA-sequencing dataset derived from hiPSC-CMs exposed to different SARS-CoV-2 concentrations (*25*) (Figure 1D). The average expression of cardiomyocyte-specific YAP target genes (*26*) in the dataset revealed that YAP targets were decreased in a dose-dependent manner after SARS-CoV-2 infection (Figure 1E). Several canonical YAP targets in cardiomyocytes are shown in Figure 1F. These data support that SARS-CoV-2 infection suppresses YAP activity in host cells.

NSP13 inhibits YAP5SA transactivation *in vitro* and *in vivo*

To identify which SARS-CoV-2 protein suppresses YAP activity, we screened 11 NSP proteins by using a dual-luciferase reporter assay. Compared with other NSPs, NSP13 strongly inhibited YAP transcription activity (Figure 2A). By using constitutively active YAP (YAP5SA), which is resistant to phosphorylation and inactivation by LATS1/2 (*27*), we found that NSP13 suppressed YAP transactivation independent of its upstream kinase LATS2 (figure supplement 2A). Moreover, NSP13 attenuated YAP5SA activity in a dose-dependent manner (Figure 2B).

To investigate NSP13 function *in vivo*, we used YAP5SA transgenic mice (aMyHC-MerCreMer;YAP5SA), which express YAP5SA in cardiomyocytes after tamoxifen administration. This induction led to cardiomyocyte hyperplasia and increased ejection fraction (EF) and fractional shortening (FS), which ultimately resulted in mortality in mice (*26*). The adenovirus expressing NSP13 (AAV9-NSP13), which specifically infects cardiomyocytes, was used in *in vivo* experiments (figure supplement 2B and Figure 2C). Expectedly, NSP13 expression in YAP5SA mouse cardiomyocytes significantly increased survival rates (Figure 2D) and restored cardiac function, as evidenced by EF and FS (Figure 2E and figure supplement S2C). Furthermore,

NSP13 expression reversed the smaller left ventricle (LV) chamber in YAP5SA mouse hearts (*26*) (Figure 2F, G). To further investigate NSP13 effects on the mouse heart, we collected heart tissue from the surviving mice 21 days after tamoxifen injection. Notably, NSP13 expression in YAP5SA mice reversed heart overgrowth (Figure 2H, I and figure supplement 2D). Overall, these data indicate that NSP13 suppresses YAP activity *in vitro* and *in vivo*.

NSP13 helicase activity is required for YAP suppression

NSP13, a helicase with conserved sequence across all coronaviruses (Figure 3A), plays a critical role in viral replication and is a promising target for antiviral treatment (*28-35*). K131, K345/K347, and R567 were identified as important amino acid sites for NSP13 helicase activity in SARS-CoV (*36*). Because of the 99.8% sequence identity of NSP13 between SARS-CoV-2 and SARS-CoV, we believed these sites were similarly crucial for SARS-CoV-2 NSP13. Reporter assays showed that NSP13-K131A with reduced helicase activity was able to suppress YAP, whereas NSP13-R567A (lost ATP consumption) and NSP13-K345A/K347A (obstructed the nucleic acid binding channel) failed to inhibit YAP activity (Figure 3B). To assess the contribution of each domain to YAP regulation, we constructed 6 NSP13 truncations (Figure 3C), but none led to a reduction in YAP transactivation (Figure 3D). These findings suggest that the full length NSP13 with helicase activity is required for to suppress YAP transactivation.

SARS-CoV-2 has consistently mutated over time, resulting in variants that differ from the original virus. We also examined the effect of the NSP13 mutations (*31*) (Figure 3E and figure supplement 3A) on YAP and found that all mutants can suppress YAP transactivation (Figure 3F and figure supplement 3A).

NSP13 interacts with TEAD4 and recruits YAP repressors into the YAP/TEAD complex

We then studied the molecular mechanism of how NSP13 suppresses YAP. Immunofluorescence data revealed that NSP13 localized in both the cytoplasm and nucleus, whereas most of YAP5SA colocalized with NSP13 in the nucleus 3 days after tamoxifen injection (Figure 4A). However, coimmunoprecipitation experiments suggested no direct interaction between NSP13 and YAP5SA (figure supplement 4A). Further investigation indicated that NSP13 associated with the transcription factor TEAD4 (Figure 4B), and both the N- and C-terminal ends of TEAD4 interacted with NSP13 (figure supplement 4B), suggesting that NSP13 may prevent YAP transactivation by competitively interacting with TEAD4. Unexpectedly, NSP13 had no effect on the YAP/TEAD4 association, but the interaction between YAP and NSP13 was much stronger in the presence of TEAD4, indicating that TEAD4 acts as a platform recruiting YAP and NSP13 (Figure 4C). Moreover, NSP13 protein levels accumulated with YAP5SA expression in cardiomyocytes (Figure 4D, E), which suggests that nuclear NSP13/YAP/TEAD4 may prevent NSP13 degradation.

Because NSP13 formed a complex with YAP/TEAD4, we hypothesized that NSP13 recruits repressors to inhibit YAP transactivation in the nucleus. The immunoprecipitation-mass spectrometry was performed to examine NSP13-interacting proteins in the presence or absence of YAP expression in HEK293T cell nuclei. We detected hundreds of candidate proteins that interact with NSP13 in the nucleus (figure supplement 4C), which were further analyzed by STRING (figure supplement 4D). Gene Ontology (GO) analysis indicated that the largest clusters are involved in RNA polymerase II transcription termination, chromatin remodeling, and protein folding (Figure 4F). We evaluated the function of a select group of these proteins in YAP transactivation by siRNA knockdown (figure supplement 4E). Reporter assay results revealed that

the siRNA knockdown of CCT3 and TTF2 increased endogenous YAP transactivation in HeLa cells (Figure 4G and figure supplement 4F), suggesting that NSP13 suppressed YAP activity by recruiting suppressors to the YAP/TEAD4 complex.

Discussion

In this study, YAP transcriptional activity was reduced after SARS-CoV-2 infection in human lung and hiPSC-CMs, and SARS-CoV-2 helicase NSP13 significantly inhibited YAP activity both *in vitro* and *in vivo*. Mechanistically, NSP13 interacted with TEAD4 and formed a complex with YAP/TEAD4 in the nucleus, which further recruited suppressors such as TTF2 and CCT3 to repress YAP-TEAD transcriptional activity (Figure 4H).

TEAD transcription factors, the major partners of YAP, are the final nuclear effectors of Hippo-YAP signaling and play critical roles in cancer development (*11,37*). In our study, NSP13 interacted with TEAD4, but did not disrupt the YAP/TEAD4 interaction, suggesting a novel regulatory mechanism for TEAD. Immunoprecipitation-mass spectrometry showed that NSP13 interacting proteins such as TTF2 and CCT3 suppressed the YAP-TEAD4 complex. TTF2, a SWI2/SNF2 family member, facilitates the removal of RNA polymerase II from the DNA template through ATP hydrolysis (*38,39*). Importantly, termination of the transcription complex elongation by TTF2 appears to be minimally affected by template position (*39*). CCT3 is a component of the chaperonin-containing T-complex, a molecular chaperone complex that facilitates protein folding upon ATP hydrolysis. In previous studies, CCT3 positively regulated the protein stability of YAP and served as a liver cancer biomarker (*40*). However, we found that the NSP13-interacting protein CCT3 inhibited YAP transactivation, suggesting a context-dependent function of CCT3 in YAP regulation. The detailed mechanisms require further study.

In conclusion, our study reveals a novel function of NSP13 in suppressing the YAP/TEAD transcriptional complex. These findings advance our understanding of the underlying effect of SARS-CoV-2 on host cells. Since it directly interacts with TEAD4 and strongly suppresses YAP transactivation, NSP13 provides a new avenue for inhibiting YAP activity as a potential treatment for YAP-driven cancer.

Materials and methods

Mice

We used αMyHC-MerCreMer mice; wild type (WT) mice and αMyHC-MerCreMer; and YAP5SA mice (*26*). Mice had a mixed genetic background of C57BL/6 and 129SV. The AAV9 virus (a total of 5×10^{11} viral genomes, 120 µl total volume) was delivered by retro-orbital injection 2 weeks before tamoxifen injection. For the survival experiment in Figure 2, two low doses of tamoxifen (10 ug/g) were administered to 6-week-old mice by intraperitoneal injection. The mouse cardiac function was evaluated by echocardiography at day 4 and day 8 post tamoxifen injection and all the surviving mice were sacrificed at day 21. For the experiments in Figure 4, two doses of tamoxifen (Figure 4A, 10 ug/g; Figure 4D-E, 50 ug/g) were injected, and the mouse hearts were collected at day 3 post tamoxifen injection.

RNA-seq analysis

For the analysis of lung samples from patients with COVID-19, snRNA sequencing data of 7 control lungs and 35 COVID-19 lungs from GSE171668 (*20*) and GSE171524 (*21*) were downloaded and analyzed using Seurat v4 software suite (*41*). A total of 223,106 nuclei were used in the analysis. Each sample was normalized, and batch corrected using SCTransformation. The mitochondrial percentage was used to regress out any technical variability between batches. We used harmony (*42*) integration to remove technical variation among the samples. The YAP score was evaluated by using 38 canonical YAP target genes. For the analysis of iPSC-CMs infected with SARS-CoV-2, bulk RNA-seq data were obtained from a study by Perez-Bermejo et al. (*25*). With this dataset, we re-analyzed and evaluated the average expression of 302 cardiomyocyte-specific YAP target genes (*26*).

Expression plasmids

Expression plasmids encoding HA-tagged WT, mutant, or truncated NSP13 were generated by polymerase chain reaction (PCR) and subcloned into pXF4H (N-terminal HA tag) derived from pRK5 (Genetech). Myc-tagged WT or truncated TEAD4, flag-tagged WT YAP, and flag-tagged YAP5SA were generated by PCR and subcloned into a pcDNA3 backbone. HA-tagged WT LATS2, LATS2 KR, and pRL-TK_Luc were gifts from Dr. Pinglong Xu's lab. Reporters of HOP-flash (#83467) and 8xGTIIC-luciferase (#34615) were purchased from Addgene. The NSP plasmids used in YAP transactivation screening experiments were gifts from Dr. Nevan J. Krogan's lab. All plasmids were confirmed by performing DNA sequencing.

Cell culture and transfection

HEK293T and HeLa cells were cultured in Dulbecco's Modified Eagle Medium with 10% fetal bovine serum. Lipofectamine™ 2000 (ThermoFisher) or Lipofectamine™ 3000 (ThermoFisher) reagents were used for plasmid transfection. LipofectAmine RNAiMAX (ThermoFisher) was used for siRNA transfection.

Luciferase reporter assay

HEK293T or HeLa cells were transfected with WT YAP- or YAP5SA responsive HOP-flash plasmid or 8xGTIIC-luciferase reporter, which has an open reading frame encoding firefly luciferase, along with the pRL-Luc with *Renilla* luciferase coding as the internal control for transfection and other expression vectors (NSPs), as specified. After 24 h of transfection with the indicated treatments, cells were lysed with passive lysis buffer (Promega). Luciferase assays were

performed by using a dual-luciferase assay kit (Promega). Data were quantified with POLARstar Omega (BMG Labtech) and normalized to the internal *Renilla* luciferase control.

AAV9 viral packaging

Viral vectors were used as previously described (*43*). The construct containing HA-tagged NSP13 was cloned into the pENN.AAV.cTNT, p1967-Q vector (AAV9-HA-NSP13). Empty vector–encoding green fluorescent protein was used as the control (AAV9-GFP). Both vectors were packaged into the muscle-trophic serotype AAV9 by the Intellectual and Developmental Disabilities Research Center Neuroconnectivity Core at Baylor College of Medicine. After being titered, viruses were aliquoted (1×10^{13} viral genome particles per tube), immediately frozen, and stored long-term at −80°C. Each aliquot was diluted in saline to make a 120-ul injection solution.

Echocardiography

Echocardiography, for cardiac function analysis, was performed on a VisualSonics Vevo 2100 system with a 550-s probe. B-mode images and M-mode images were captured on a short-axis projection. Ejection fraction, fractional shortening, diameter of diastolic left ventricle, diameter of systolic left ventricle, and end-diastolic volume were calculated by using a cardiac measurement package installed in the Vevo2100 system.

Histology and Immunofluorescence staining

Hearts were fixed in 4% paraformaldehyde overnight at 4 °C, dehydrated in serial ethanol and xylene solutions, and embedded in paraffin. For immunofluorescence staining, slides were sectioned at 7-μm intervals. For paraffin sections, samples were deparaffinized and rehydrated,

treated with 3% H_2O_2 in EtOH and then with antigen retrieval solution (Vector Laboratories Inc., Burlingame, CA, USA), blocked with 10% donkey serum in phosphate-buffered saline, and incubated with primary antibodies. The antibodies used were rabbit anti-HA (#3724, Cell signaling) and rat anti-flag (NBP1-06712, Novus Bio-logicals). Immunofluorescence stained images were captured on a Zeiss LSM 780 NLO Confocal/2-hoton microscope.

Statistical Analysis

For the data in our manuscript, the specific statistical test used is presented in the figure legend. In snRNA-seq analyses, Yap score difference between AT1 from Control and COVID19 patients was identified by using Wilcoxon test. For the analysis of iPSC-CMs infected with SARS-CoV-2, the expression score of cardiomyocyte YAP targets was evaluated by Student t-test. The mice survival rate in Figure 2D was analyzed by log-rank (Mantel-Cox) test. For the other cardiac data, including EF, FS and Diameter of systolic LV, the statistical significance of the observed differences was evaluated by using three-way ANOVA and the Šídák's multiple comparisons test. For all the reporter assays in cells and heart/body ratio in Figure S2E, the statistical significance of the observed differences in mean was evaluated by using a one-way or two-way ANOVA and the post hoc Tukey's multiple comparisons test. The P value less than 0.05 was considered statistically significant (*$p< 0.05$, **$p< 0.01$, ***$p< 0.001$, ****$p< 0.0001$).

References

1. S. Ma, Z. Meng, R. Chen, K. L. Guan, The Hippo pathway: Biology and pathophysiology. *Annu. Rev. Biochem.* **88**, 577-604 (2019).

2. J. Wang, S. Liu, T. Heallen, J. F. Martin, The Hippo pathway in the heart: pivotal roles in development, disease, and regeneration. *Nat. Rev. Cardiol* **15**, 672-684 (2018).

3. F. Meng, B. Xie, J. F. Martin, Targeting the Hippo pathway in heart repair. *Cardiovasc. Res.* **118**, 2402-2414 (2022).

4. J. O. Russell, F. D. Camargo, Hippo signalling in the liver: role in development, regeneration and disease. *Nat. Rev. Gastroenterol. Hepatol.* **19**, 297-312 (2022).

5. A. W. Hong, Z. Meng, K. L. Guan, The Hippo pathway in intestinal regeneration and disease. *Nat. Rev. Gastroenterol. Hepatol.* **13**, 324-337 (2016).

6. I. M. Moya, G. Halder, Hippo-YAP/TAZ signalling in organ regeneration and regenerative medicine. *Nat. Rev. Mol. Cell Biol.* **20**, 211-226 (2019).

7. Y. Zhang, H. Zhang, B. Zhao, Hippo signaling in the immune system. *Trends Biochem. Sci.* **43**, 77-80 (2018).

8. S. Paul, S. Xie, X. Yao, A. Dey, Transcriptional regulation of the hippo pathway: Current understanding and insights from single-cell technologies. *Cells* **11**, (2022).

9. A. Pocaterra, P. Romani, S. Dupont, YAP/TAZ functions and their regulation at a glance. *J. Cell Sci.* **133**, (2020).

10. K. C. Lin, H. W. Park, K. L. Guan, Regulation of the Hippo pathway transcription factor TEAD. *Trends Biochem. Sci.* **42**, 862-872 (2017).

11. H. D. Huh, D. H. Kim, H. S. Jeong, H. W. Park, Regulation of TEAD transcription factors in cancer biology. *Cells* **8**, (2019).

12. S. Wang, F. Xie, F. Chu, Z. Zhang, B. Yang, T. Dai, L. Gao, L. Wang, L. Ling, J. Jia, H. van Dam, J. Jin, L. Zhang, F. Zhou, YAP antagonizes innate antiviral immunity and is targeted for lysosomal degradation through IKKvarepsilon-mediated phosphorylation. *Nat. Immunol.* **18**, 733-743 (2017).

13. Q. Zhang, F. Meng, S. Chen, S. W. Plouffe, S. Wu, S. Liu, X. Li, R. Zhou, J. Wang, B. Zhao, J. Liu, J. Qin, J. Zou, X. H. Feng, K. L. Guan, P. Xu, Hippo signalling governs cytosolic nucleic acid sensing through YAP/TAZ-mediated TBK1 blockade. *Nat. Cell Biol.* **19**, 362-374 (2017).

14. Z. Wang, W. Lu, Y. Zhang, F. Zou, Z. Jin, T. Zhao, The Hippo pathway and viral infections. *Front Microbiol* **10**, 3033 (2019).

15. C. Ma, Y. Cong, H. Zhang, COVID-19 and the digestive system. *Am. J. Gastroenterol.* **115**, 1003-1006 (2020).

16. F. G. De Felice, F. Tovar-Moll, J. Moll, D. P. Munoz, S. T. Ferreira, Severe acute respiratory syndrome coronavirus 2 (SARS-CoV-2) and the central nervous system. *Trends Neurosci.* **43**, 355-357 (2020).

17. M. Nishiga, D. W. Wang, Y. Han, D. B. Lewis, J. C. Wu, COVID-19 and cardiovascular disease: from basic mechanisms to clinical perspectives. *Nat. Rev. Cardiol* **17**, 543-558 (2020).

18. G. Garcia, Jr., A. V. Jeyachandran, Y. Wang, J. I. Irudayam, S. C. Cario, C. Sen, S. Li, Y. Li, A. Kumar, K. Nielsen-Saines, S. W. French, P. S. Shah, K. Morizono, B. N. Gomperts, A. Deb, A. Ramaiah, V. Arumugaswami, Hippo signaling pathway activation during SARS-CoV-2 infection contributes to host antiviral response. *PLoS Biol.* **20**, e3001851 (2022).

19. S. M. Pinto, Y. Subbannayya, H. Kim, L. Hagen, M. W. Gorna, A. I. Nieminen, M. Bjoras, T. Espevik, D. Kainov, R. K. Kandasamy, Multi-OMICs landscape of SARS-CoV-2-induced host responses in human lung epithelial cells. *iScience* **26**, 105895 (2023).

20. T. M. Delorey, C. G. K. Ziegler, G. Heimberg, R. Normand, Y. Yang, A. Segerstolpe, D. Abbondanza, S. J. Fleming, A. Subramanian, D. T. Montoro, K. A. Jagadeesh, K. K. Dey, P. Sen, M. Slyper, Y. H. Pita-Juarez, D. Phillips, J. Biermann, Z. Bloom-Ackermann, N. Barkas, A. Ganna, J. Gomez, J. C. Melms, I. Katsyv, E. Normandin, P. Naderi, Y. V. Popov, S. S. Raju, S. Niezen, L. T. Tsai, K. J. Siddle, M. Sud, V. M. Tran, S. K. Vellarikkal, Y. Wang, L. Amir-Zilberstein, D. S. Atri, J. Beechem, O. R. Brook, J. Chen, P. Divakar, P. Dorceus, J. M. Engreitz, A. Essene, D. M. Fitzgerald, R. Fropf, S. Gazal, J. Gould, J. Grzyb, T. Harvey, J. Hecht, T. Hether, J. Jane-Valbuena, M. Leney-Greene, H. Ma, C. McCabe, D. E. McLoughlin, E. M. Miller, C. Muus, M. Niemi, R. Padera, L. Pan, D. Pant, C. Pe'er, J. Pfiffner-Borges, C. J. Pinto, J. Plaisted, J. Reeves, M. Ross, M. Rudy, E. H. Rueckert, M. Siciliano, A. Sturm, E. Todres, A. Waghray, S. Warren, S. Zhang, D. R. Zollinger, L. Cosimi, R. M. Gupta, N. Hacohen, H. Hibshoosh, W. Hide, A. L. Price, J. Rajagopal, P. R. Tata, S. Riedel, G. Szabo, T. L. Tickle, P. T. Ellinor, D. Hung, P. C. Sabeti, R. Novak, R. Rogers, D. E. Ingber, Z. G. Jiang, D. Juric, M. Babadi, S. L. Farhi, B. Izar, J. R. Stone, I. S. Vlachos, I. H. Solomon, O. Ashenberg, C. B. M. Porter, B. Li, A. K. Shalek, A. C. Villani, O. Rozenblatt-Rosen, A. Regev, COVID-19 tissue atlases reveal SARS-CoV-2 pathology and cellular targets. *Nature* **595**, 107-113 (2021).

21. J. C. Melms, J. Biermann, H. Huang, Y. Wang, A. Nair, S. Tagore, I. Katsyv, A. F. Rendeiro, A. D. Amin, D. Schapiro, C. J. Frangieh, A. M. Luoma, A. Filliol, Y. Fang, H. Ravichandran, M. G. Clausi, G. A. Alba, M. Rogava, S. W. Chen, P. Ho, D. T. Montoro,

A. E. Kornberg, A. S. Han, M. F. Bakhoum, N. Anandasabapathy, M. Suarez-Farinas, S. F. Bakhoum, Y. Bram, A. Borczuk, X. V. Guo, J. H. Lefkowitch, C. Marboe, S. M. Lagana, A. Del Portillo, E. J. Tsai, E. Zorn, G. S. Markowitz, R. F. Schwabe, R. E. Schwartz, O. Elemento, A. Saqi, H. Hibshoosh, J. Que, B. Izar, A molecular single-cell lung atlas of lethal COVID-19. *Nature* **595**, 114-119 (2021).

22. M. Hoffmann, H. Kleine-Weber, S. Schroeder, N. Kruger, T. Herrler, S. Erichsen, T. S. Schiergens, G. Herrler, N. H. Wu, A. Nitsche, M. A. Muller, C. Drosten, S. Pohlmann, SARS-CoV-2 cell entry depends on ACE2 and TMPRSS2 and is blocked by a clinically proven protease inhibitor. *Cell* **181**, 271-280 e278 (2020).

23. I. J. Penkala, D. C. Liberti, J. Pankin, A. Sivakumar, M. M. Kremp, S. Jayachandran, J. Katzen, J. P. Leach, R. Windmueller, K. Stolz, M. P. Morley, A. Babu, S. Zhou, D. B. Frank, E. E. Morrisey, Age-dependent alveolar epithelial plasticity orchestrates lung homeostasis and regeneration. *Cell Stem Cell* **28**, 1775-1789 e1775 (2021).

24. J. J. Gokey, J. Snowball, A. Sridharan, P. Sudha, J. A. Kitzmiller, Y. Xu, J. A. Whitsett, YAP regulates alveolar epithelial cell differentiation and AGER via NFIB/KLF5/NKX2-1. *iScience* **24**, 102967 (2021).

25. J. A. Perez-Bermejo, S. Kang, S. J. Rockwood, C. R. Simoneau, D. A. Joy, A. C. Silva, G. N. Ramadoss, W. R. Flanigan, P. Fozouni, H. Li, P. Y. Chen, K. Nakamura, J. D. Whitman, P. J. Hanson, B. M. McManus, M. Ott, B. R. Conklin, T. C. McDevitt, SARS-CoV-2 infection of human iPSC-derived cardiac cells reflects cytopathic features in hearts of patients with COVID-19. *Sci. Transl. Med.* **13**, (2021).

26. T. O. Monroe, M. C. Hill, Y. Morikawa, J. P. Leach, T. Heallen, S. Cao, P. H. L. Krijger, W. de Laat, X. H. T. Wehrens, G. G. Rodney, J. F. Martin, YAP partially reprograms

chromatin accessibility to directly induce adult cardiogenesis in vivo. *Dev. Cell* **48**, 765-779 e767 (2019).

27. B. Zhao, X. Wei, W. Li, R. S. Udan, Q. Yang, J. Kim, J. Xie, T. Ikenoue, J. Yu, L. Li, P. Zheng, K. Ye, A. Chinnaiyan, G. Halder, Z. C. Lai, K. L. Guan, Inactivation of YAP oncoprotein by the Hippo pathway is involved in cell contact inhibition and tissue growth control. *Genes Dev.* **21**, 2747-2761 (2007).

28. L. Yan, J. Ge, L. Zheng, Y. Zhang, Y. Gao, T. Wang, Y. Huang, Y. Yang, S. Gao, M. Li, Z. Liu, H. Wang, Y. Li, Y. Chen, L. W. Guddat, Q. Wang, Z. Rao, Z. Lou, Cryo-EM structure of an extended SARS-CoV-2 replication and transcription complex reveals an intermediate state in cap synthesis. *Cell* **184**, 184-193 e110 (2021).

29. J. Chen, B. Malone, E. Llewellyn, M. Grasso, P. M. M. Shelton, P. D. B. Olinares, K. Maruthi, E. T. Eng, H. Vatandaslar, B. T. Chait, T. M. Kapoor, S. A. Darst, E. A. Campbell, Structural basis for helicase-polymerase coupling in the SARS-CoV-2 replication-transcription complex. *Cell* **182**, 1560-1573 e1513 (2020).

30. L. Yan, Y. Zhang, J. Ge, L. Zheng, Y. Gao, T. Wang, Z. Jia, H. Wang, Y. Huang, M. Li, Q. Wang, Z. Rao, Z. Lou, Architecture of a SARS-CoV-2 mini replication and transcription complex. *Nat. Commun.* **11**, 5874 (2020).

31. J. A. Newman, A. Douangamath, S. Yadzani, Y. Yosaatmadja, A. Aimon, J. Brandao-Neto, L. Dunnett, T. Gorrie-Stone, R. Skyner, D. Fearon, M. Schapira, F. von Delft, O. Gileadi, Structure, mechanism and crystallographic fragment screening of the SARS-CoV-2 NSP13 helicase. *Nat. Commun.* **12**, 4848 (2021).

32. J. Chen, Q. Wang, B. Malone, E. Llewellyn, Y. Pechersky, K. Maruthi, E. T. Eng, J. K. Perry, E. A. Campbell, D. E. Shaw, S. A. Darst, Ensemble cryo-EM reveals conformational

states of the nsp13 helicase in the SARS-CoV-2 helicase replication-transcription complex. *Nat. Struct. Mol. Biol.* **29**, 250-260 (2022).

33. B. Malone, J. Chen, Q. Wang, E. Llewellyn, Y. J. Choi, P. D. B. Olinares, X. Cao, C. Hernandez, E. T. Eng, B. T. Chait, D. E. Shaw, R. Landick, S. A. Darst, E. A. Campbell, Structural basis for backtracking by the SARS-CoV-2 replication-transcription complex. *Proc Natl Acad Sci U S A* **118**, (2021).

34. R. Nandi, D. Bhowmik, R. Srivastava, A. Prakash, D. Kumar, Discovering potential inhibitors against SARS-CoV-2 by targeting Nsp13 Helicase. *J. Biomol. Struct. Dyn.* **40**, 12062-12074 (2022).

35. J. Zeng, F. Weissmann, A. P. Bertolin, V. Posse, B. Canal, R. Ulferts, M. Wu, R. Harvey, S. Hussain, J. C. Milligan, C. Roustan, A. Borg, L. McCoy, L. S. Drury, S. Kjaer, J. McCauley, M. Howell, R. Beale, J. F. X. Diffley, Identifying SARS-CoV-2 antiviral compounds by screening for small molecule inhibitors of nsp13 helicase. *Biochem. J.* **478**, 2405-2423 (2021).

36. Z. Jia, L. Yan, Z. Ren, L. Wu, J. Wang, J. Guo, L. Zheng, Z. Ming, L. Zhang, Z. Lou, Z. Rao, Delicate structural coordination of the severe acute respiratory syndrome coronavirus Nsp13 upon ATP hydrolysis. *Nucleic Acids Res.* **47**, 6538-6550 (2019).

37. A. V. Pobbati, R. Kumar, B. P. Rubin, W. Hong, Therapeutic targeting of TEAD transcription factors in cancer. *Trends Biochem. Sci.* **48**, 450-462 (2023).

38. M. Liu, Z. Xie, D. H. Price, A human RNA polymerase II transcription termination factor is a SWI2/SNF2 family member. *J. Biol. Chem.* **273**, 25541-25544 (1998).

39. Y. Jiang, M. Liu, C. A. Spencer, D. H. Price, Involvement of transcription termination factor 2 in mitotic repression of transcription elongation. *Mol. Cell* **14**, 375-385 (2004).

40. Y. Liu, X. Zhang, J. Lin, Y. Chen, Y. Qiao, S. Guo, Y. Yang, G. Zhu, Q. Pan, J. Wang, F. Sun, CCT3 acts upstream of YAP and TFCP2 as a potential target and tumour biomarker in liver cancer. *Cell Death Dis.* **10**, 644 (2019).

41. Y. Hao, S. Hao, E. Andersen-Nissen, W. M. Mauck, 3rd, S. Zheng, A. Butler, M. J. Lee, A. J. Wilk, C. Darby, M. Zager, P. Hoffman, M. Stoeckius, E. Papalexi, E. P. Mimitou, J. Jain, A. Srivastava, T. Stuart, L. M. Fleming, B. Yeung, A. J. Rogers, J. M. McElrath, C. A. Blish, R. Gottardo, P. Smibert, R. Satija, Integrated analysis of multimodal single-cell data. *Cell* **184**, 3573-3587 e3529 (2021).

42. I. Korsunsky, N. Millard, J. Fan, K. Slowikowski, F. Zhang, K. Wei, Y. Baglaenko, M. Brenner, P. R. Loh, S. Raychaudhuri, Fast, sensitive and accurate integration of single-cell data with Harmony. *Nat. Methods* **16**, 1289-1296 (2019).

43. J. P. Leach, T. Heallen, M. Zhang, M. Rahmani, Y. Morikawa, M. C. Hill, A. Segura, J. T. Willerson, J. F. Martin, Hippo pathway deficiency reverses systolic heart failure after infarction. *Nature* **550**, 260-264 (2017).

Acknowledgments

We are grateful to Drs. Nevan J. Krogan and Pinglong Xu for the gift of plasmids. Dr. Hongxin Guan helped with NSP13 mutant structure analysis. Rebecca Bartow, PhD, of the Department of Scientific Publications at The Texas Heart Institute, provided editorial support.

Funding

National Institutes of Health grant HL 127717 (JFM).

National Institutes of Health grant HL 130804 (JFM).

National Institutes of Health grant HL 118761 (JFM).

Vivian L. Smith Foundation (JFM).

2020 COVID-19 RFA (JFM).

AHA postdoctoral fellowship 903411 (FM).

AHA postdoctoral fellowship 903651 (RL).

K99 HL169742 (JS)

Don McGill Gene Editing Laboratory of The Texas Heart Institute (XL).

Author contributions

Conceptualization: FM, JFM

Methodology: JK, JS, XL

Investigation: FM, C-RT, JW, YS, VD, BX, RL, SL

Supervision: JFM

Writing – original draft: FM

Writing – review & editing: FM, JFM

Data and materials availability

All data are available in the main text or the supplementary materials.

Figures and Figure Legends

Figure 1

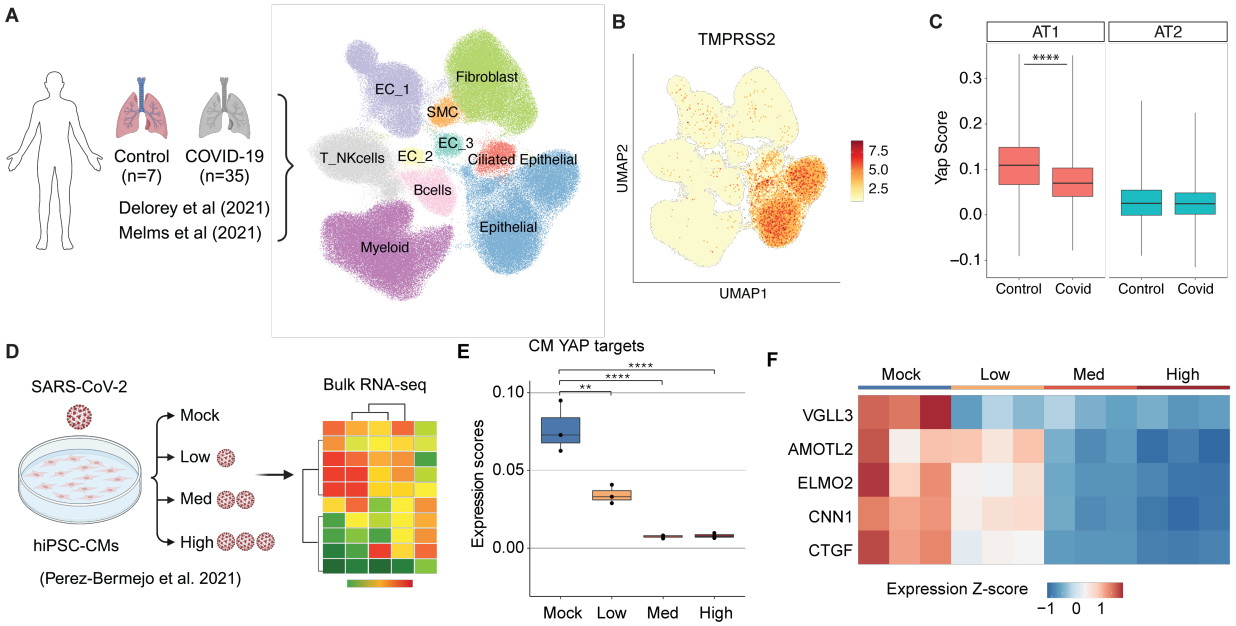

Figure 1. SARS-CoV-2 infection suppresses YAP activity *in vivo* and *in vitro*. (**A**) Overview of integrated single-nucleus RNA sequencing and uniform manifold approximation and projection (UMAP) of cell types in lung samples from controls and patients with COVID-19. EC, endothelial cells; NK, natural killer cells; SMC, smooth muscle cells. (**B**) UMAP visualization of TMPRESS2 expression in the 10 cell types. (**C**) Yap scores in alveolar type 1 (AT1) and alveolar type 2 (AT2) epithelial cells from lung samples in controls and patients with COVID-19. Wilcoxon test, ****p< 0.0001. (**D**) Overview of SARS-CoV-2 infection in human induced pluripotent stem cell–derived cardiomyocytes (hiPSC-CMs). (**E**) Box plot showing the mean expression scores of known YAP target genes in hiPSC-CM bulk RNA-sequencing data. Each dot represents a biological replicate. Student *t*-test;**p< 0.01, ****p< 0.0001. (**F**) Heatmap displaying the expression Z-scores of example YAP targets in the iPSC-CM bulk RNA-sequencing data. Each column corresponds to a single biological sample.

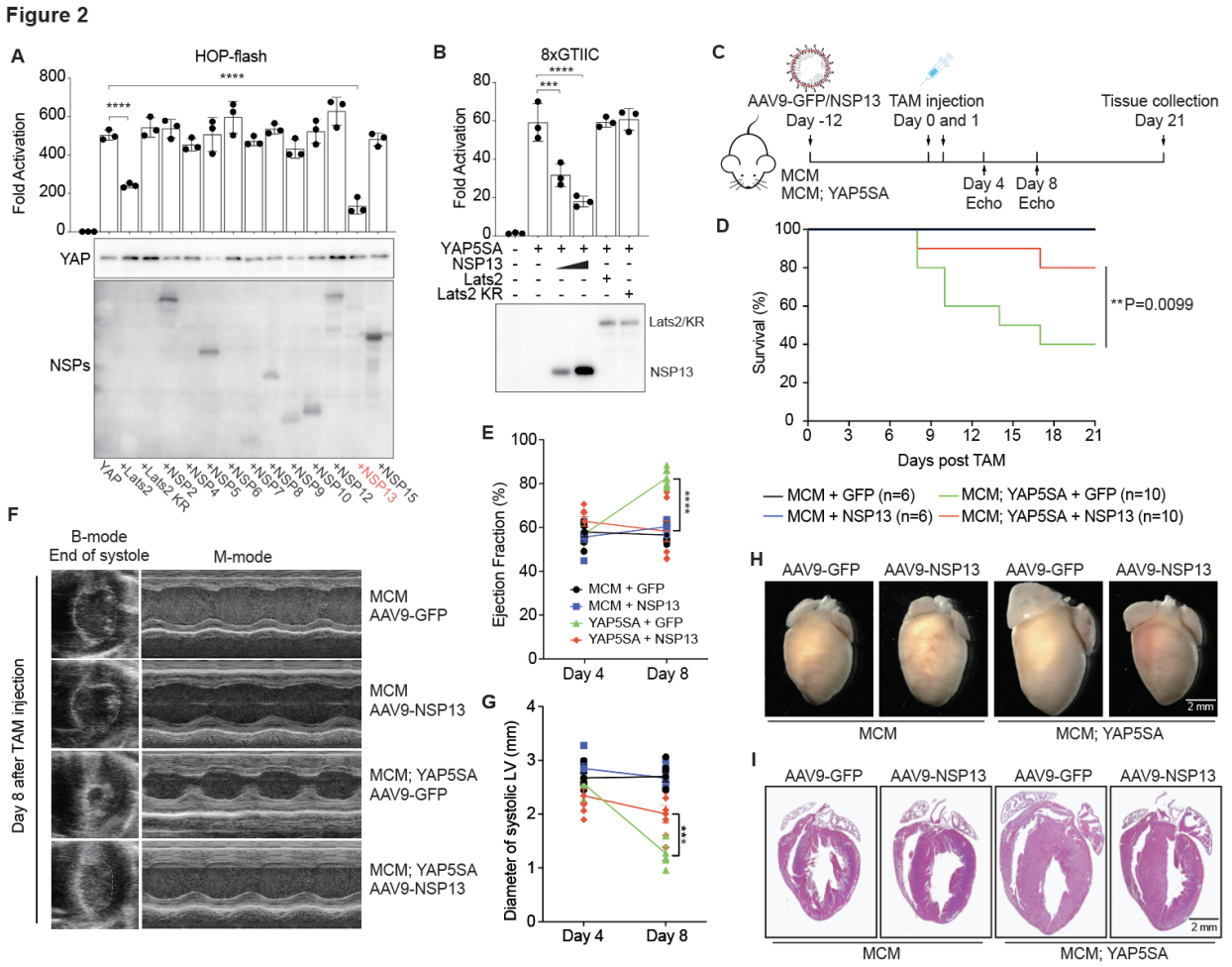

Figure 2. NSP13 inhibits YAP transactivation *in vitro* and *in vivo*. (**A**) Screening of 11 NSPs for YAP activation by using a dual-luciferase reporter assay (HOP-flash). Compared with other NSPs, NSP13 strongly inhibited YAP transactivation at low levels of protein expression. (n = 3 independent experiments; data are reported as mean ± SD). ****p< 0.0001, one-way ANOVA. (**B**) Reporter assay (8xGTIIC) results showing that NSP13 but not YAP upstream kinase LATS2 inhibited YAP5SA transactivation in a dose-dependent manner. (n = 3 independent experiments; data are presented as the mean ± SD). ***p< 0.001, ****p< 0.0001, one-way ANOVA. (**C**) Experimental design of NSP13 study in mice. Both Control (aMyHC-MerCreMer;WT) and YAP5SA (aMyHC-MerCreMer;YAP 5SA) mice were injected with AAV9-GFP or AAV9-NSP13. At 12 days after virus injection, the mice received two low-dose of TAM (10 ug/g).

Cardiac function was recorded by echocardiography at day 4 and 8 after the second shot of tamoxifen. The mouse hearts of all the surviving mice were collected at day 21 post tamoxifen injection. (**D**) NSP13 expression in cardiomyocytes improved survival rate of YAP5SA mice after TAM injection compared to YAP5SA mice with AAV9-GFP infection. **p=0.0099, log-rank (Mantel-Cox) test. (**E**) Ejection fraction in YAP5SA mice was increased on day 8 after tamoxifen injections (10 ug/g x2). NSP13 expression reversed the increase of EF in YAP5SA mice. ****p<0.0001, three-way ANOVA. (**F**) Representative B-mode and M-mode echocardiographic images of mouse hearts in four groups 8 days after tamoxifen (TAM) induction. (**G**) A reduction in the size of the left ventricle was seen in YAP5SA mice at day 8 after tamoxifen injection. NSP13 introduction reversed this trend as evidenced by an increase in the diameter of the left ventricle. ***p< 0.001, three-way ANOVA. (**H-I**) Representative whole mount and hematoxylin & eosin images of mouse hearts at 21 days after tamoxifen induction. Scale bar, 2 mm.

Figure 3

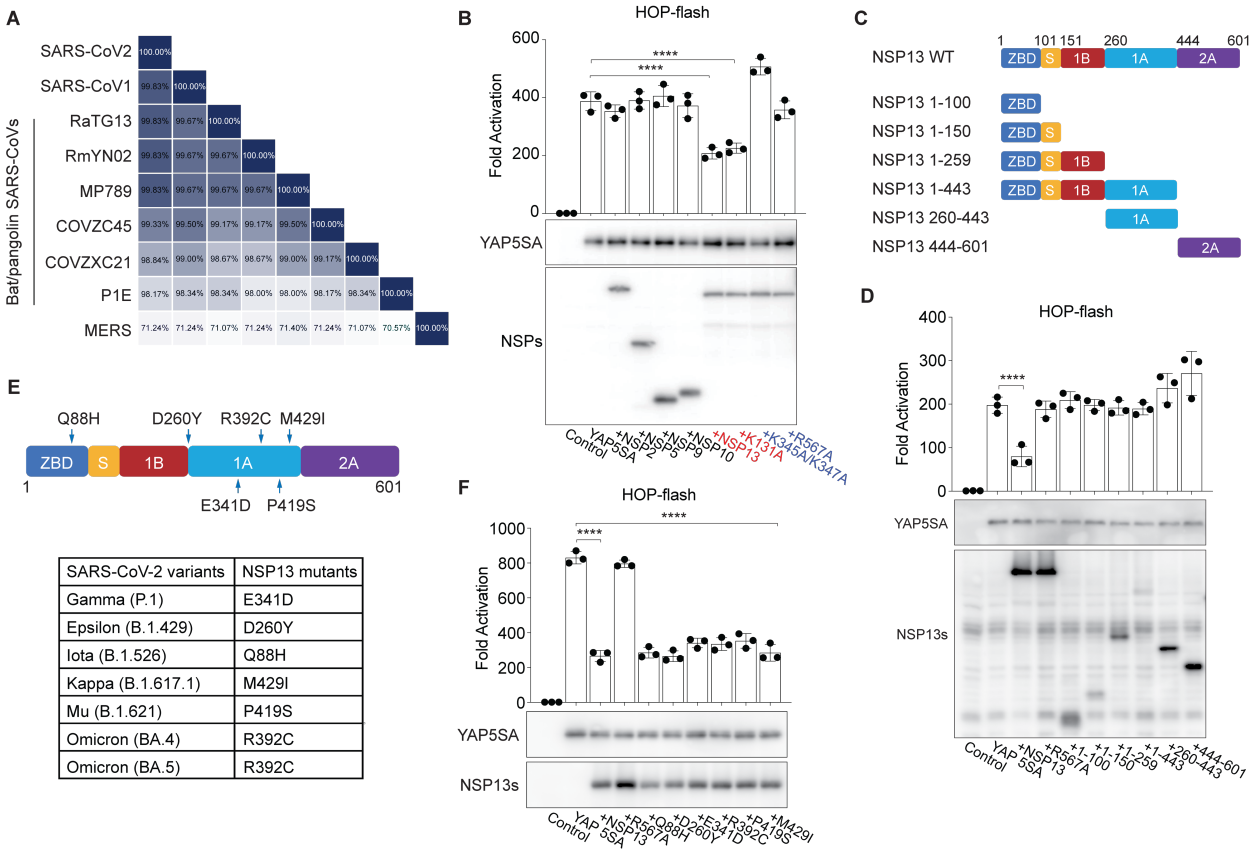

SARS-CoV-2 variants	NSP13 mutants
Gamma (P.1)	E341D
Epsilon (B.1.429)	D260Y
Iota (B.1.526)	Q88H
Kappa (B.1.617.1)	M429I
Mu (B.1.621)	P419S
Omicron (BA.4)	R392C
Omicron (BA.5)	R392C

Figure 3. NSP13 helicase activity is required for suppressing YAP activity. (**A**) Conserved amino acid sequences of NSP13 among coronaviruses. (**B**) We constructed SARS-CoV-2 NSP13 mutant plasmids to examine the mechanisms underlying YAP suppression. NSP13-R567A, which loses its ATP consumption ability, did not inhibit YAP5SA transactivation, whereas NSP13 K345A/K347A, which loses its nucleic acid binding activity, mildly promoted YAP5SA transactivation. (n = 3 independent experiments; data are reported as the mean ± SD). **$p < 0.01$, ****$p < 0.0001$, one-way ANOVA. (**C**) We constructed 6 NSP13 truncations on the basis of the NSP13 domain map. (**D**) Reporter assay results indicated that none of the truncations led to a reduction in YAP transactivation and the NSP13 DNA binding domains 1A and 2A slightly increased YAP5SA activation, suggesting that the full length NSP13 with helicase activity may be required for suppression of YAP transactivation. (n = 3 independent experiments; data are reported

as the mean ± SD). *$p < 0.05$, ****$p<0.0001$, one-way ANOVA. (**E**) Summary of NSP13 mutants from SARS-CoV2 variants. (**F**) Reporter assay (HOP-flash) results indicated that NSP13 mutations did not affect its suppression of YAP5SA transactivation. ****$p < 0.0001$, one-way ANOVA.

Figure. 4

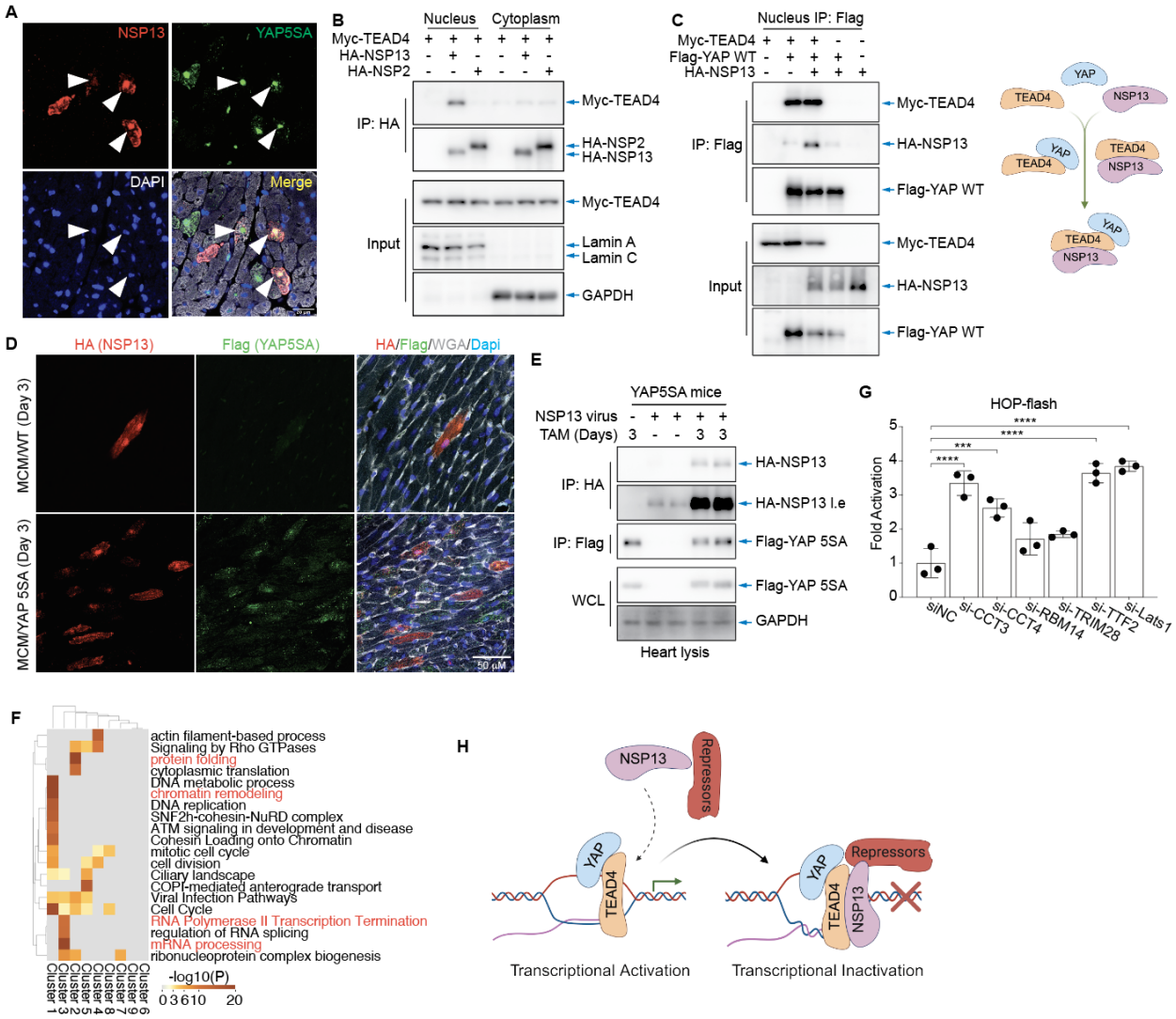

Figure 4. NSP13 inactivates the YAP/TEAD4 complex by recruiting YAP repressors. (**A**) Immunofluorescence imaging showing that NSP13 colocalized with YAP5SA in cardiomyocytes of YAP5SA transgenic mice 3 days after tamoxifen injection. (**B**) Co-immunoprecipitation results suggesting that NSP13 interacts with TEAD4, a major binding partner of YAP, in the nucleus. (**C**) Results of co-immunoprecipitation experiments in nucleus of HEK293T cells showing that NSP13 did not disrupt the interaction between YAP and TEAD4, whereas TEAD4 promoted the interaction between YAP and NSP13. A working model for the YAP/TEAD4/NSP13 complex is that TEAD4 acts as a platform for recruiting YAP and NSP13. (**D-E**) Immunofluorescence

imaging and western blot analysis showing that NSP13 protein levels increased after YAP5SA expression in cardiomyocytes of YAP5SA transgenic mice. (**F**) GO analysis in subclusters of NSP13 interacting proteins (SAINT, AvgP >0.6, labelled with red in Figure S4C). (**G**) Reporter assay (HOP-flash) results showed that endogenous YAP activity was increased after the siRNA-mediated knockdown of CCT3 and TTF2 in HeLa cells. ***$p < 0.001$, ****$p < 0.0001$, one-way ANOVA. (**H**) Working model: NSP13, together with its interacting proteins (YAP-TEAD repressors), are recruited to the YAP/TEAD complex by interacting with TEAD4, which results in YAP-TEAD inactivation.